Taylor & Francis
Taylor & Francis Group

Computer Methods in Biomechanics and Biomedical Engineering

ISSN: 1025-5842 (Print) 1476-8259 (Online) Journal homepage: http://www.tandfonline.com/loi/gcmb20

An Eulerian/XFEM formulation for the large deformation of cortical cell membrane

Franck J. Vernerey & Mehdi Farsad

To cite this article: Franck J. Vernerey & Mehdi Farsad (2011) An Eulerian/XFEM formulation for the large deformation of cortical cell membrane, Computer Methods in Biomechanics and Biomedical Engineering, 14:05, 433-445, DOI: 10.1080/10255842.2010.531273

To link to this article: https://doi.org/10.1080/10255842.2010.531273

Computer Methods in Biomechanics and Biomedical Engineering
Vol. 14, No. 5, May 2011, 433–445

Taylor & Francis
Taylor & Francis Group

An Eulerian/XFEM formulation for the large deformation of cortical cell membrane

Franck J. Vernerey* and Mehdi Farsad

Department of Civil, Environmental and Architectural Engineering, University of Colorado at Boulder, Boulder, CO 80309-0428, USA

(*Received 6 August 2010; final version received 8 October 2010*)

Most animal cells are surrounded by a thin layer of actin meshwork below their membrane, commonly known as the actin cortex (or cortical membrane). An increasing number of studies have highlighted the role of this structure in many cell functions including contraction and locomotion, but modelling has been limited by the fact that the membrane thickness (about 1 μm) is usually much smaller than the typical size of a cell (10–100 μm). To overcome theoretical and numerical issues resulting from this observation, we introduce in this paper a continuum formulation, based on surface elasticity, that views the cortex as an infinitely thin membrane that can resists tangential deformation. To accurately model the large deformations of cells, we introduced equilibrium equations and constitutive relations within the Eulerian viewpoint such that all quantities (stress, rate of deformation) lie in the current configuration. A solution procedure is then introduced based on a coupled extended finite element approach that enables a continuum solution to the boundary value problem in which discontinuities in both strain and displacement (due to cortical elasticity) are easily handled. We validate the approach by studying the effect of cortical elasticity on the deformation of a cell adhering on a stiff substrate and undergoing internal contraction. Results show very good prediction of the proposed method when compared with experimental observations and analytical solutions for simple cases. In particular, the model can be used to study how cell properties such as stiffness and contraction of both cytoskeleton and cortical membrane lead to variations in cell's surface curvature. These numerical results show that the proposed method can be used to gain critical insights into how the cortical membrane affects cell deformation and how it may be used as a means to determine a cell's mechanical properties by measuring curvatures of its membrane.

Keywords: cell deformation; cortical membrane; surface elasticity; extended finite element method

1. Introduction

Functions and health of biological tissues such as skin, cartilage and cardiac tissues rely on the interaction between population of cells (e.g. fibroblasts and chondrocytes) and their surrounding fibrous extracellular matrix (ECM). These interactions strongly depend on many internal characteristics, including ECM and cell properties, deformation and orientation, as well as on external factors such as the existence of external loads and their variation in time (Schwarz and Bischofs 2005). Any change in cell behaviour and morphology (due to disease, for instance), ECM properties and structure (from ageing or injuries) or external forces affects the mechanical and chemical equilibrium of tissues. This may result in significant consequences, including tissue remodelling and reorganisation (Harris et al. 1980), change in cell phenotype, angiogenesis (Butcher et al. 2009) or apoptosis (Wang et al. 2000; Levental et al. 2006). Research advances will depend on our ability to characterise and predict the very factors that determine cell shapes in various environments. In this quest, the derivation of accurate mechanical models of cell deformation plays a key role. Traditionally, research on cell mechanics has concentrated on the deformation of the cytoplasm (that comprises the cytoskeleton and the cytosol) for which three main families of models were developed: structural models, polymer-based models and multiphasic models. Structural models, such as the tensegrity model (Stamenovic et al. 1996; Wang et al. 2001; Ingber 2003a, 2003b), have been successful at relating the general deformation of cells to the nature of their individual components, including actin filaments and microtubules. In contrast, continuum models such as polymer-based theories (MacKintosh et al. 1995) and biphasic mixtures (Guilak et al. 2002; Ateshian et al. 2006) provide a less precise but more flexible platform for the description of a wider range of phenomena. For instance, polymer-based models are able to explain the inherent stress stiffening of the cytoskeleton filament network measured in experiments (MacKintosh et al. 1995), whereas biphasic models are ideal to describe the flow-dependent behaviour of the cytoplasm (Ateshian et al. 2006).

In addition to the cytoplasm, recent studies have highlighted the role of the cortical membrane on cell deformation. This important component of the cell's cytoskeleton can be described as a dense layer of actin bundles beneath the surface membrane (Hogan and Feeney 1963; Stehbens 1966) that acts as a protective layer against

*Corresponding author. Email: franck.vernerey@colorado.edu

ISSN 1025-5842 print/ISSN 1476-8259 online

DOI: 10.1080/10255842.2010.531273
http://www.informaworld.com

cell damage. This thin actin layer is also known to play a large role during cell migration in 3D environments by initiating bleb formation on the surface of cells (Dai and Sheetz 1999; Fackler and Grosse 2008; Tinevez et al. 2009). A number of models were proposed to better understand the behaviour of the cortical membrane and its role in cell morphology. Hansen et al. (1996, 1997) developed a numerical network model to establish a connection between the elasticity of red blood cell membrane and its random molecular structure. Other relevant studies include the work of Bar-Ziv et al. (1999) on the phenomenon of pearling caused by mechanical interactions between the surface tension and the elasticity of the actin cortex below the membrane (Hartwig and Shevlin 1986; Keller and Eggli 1998). In this approach, a simple model based on a line tension approximation of cortical membrane elasticity provided good prediction of cell shape in different environments. This was followed by the work of Bischofs et al. (2008), in which the authors derived an analytical model based on Laplace's law to investigate the influence of the cortical membrane on the shape of contractile fibroblasts attached to periodically distributed adhesion islands. By comparing their model with experimental observations, they showed that the method could predict the magnitude of the membrane curvature for cells of different sizes. Although the aforementioned studies concentrated on the role of cortical membrane only, the properties of the (bulk) cytoskeleton are also known to play a significant role on cell morphology. Accurate mechanical models of cells should, therefore, consider the combined effects of bulk cytoskeleton and cortex elasticity. However, from a computational viewpoint, the difference of length scales between a cell ($50-500\,\mu m$) and its cortical membrane thickness (less than a micron) poses a challenge that is inherent to most multiscale problems (Vernerey, Liu and Moran 2007; Vernerey, Liu, Moran and Olson 2007, 2009), providing an accurate description of the cortical membrane on the length scale of a single cell results in a very expensive numerical problem and vice versa. This may explain why existing models of cell deformation have neither considered the cortical membrane nor presented a coarse description of it (Unnikrishnan and Unnikrishnan 2007).

To overcome this issue, we in this study propose to consider the actin cortex as a 2D membrane, of negligible thickness, surrounding the cell. In this context, modelling cortical membrane mechanics can be cast within the framework of surface elasticity, originally introduced by Gurtin (1998). Existing work on surface elasticity has traditionally concentrated on surface effects in nanomaterials (Yvonnet et al. 2008; Farsad et al. 2010) in the context of infinitesimal deformation. However, because cell deformation can be quite significant in many applications, a contribution of this paper is to extend the surface elasticity formulation in the case of large deformation and to investigate its predictive power on the influence of cortical membrane on cell deformation. The equations of surface elasticity are, therefore, redefined in the general case of large deformation, following an Eulerian approach. As such, we develop the equation of equilibrium for the general case of a cell embedded in a matrix, for which the effect of the cortical membrane is important. A numerical strategy, based on the extended finite element method (XFEM), is then introduced in order to solve the system of coupled partial differential equations. The presented method possesses the following advantages. First, the presented framework uses Eulerian formulation that is suitable for large deformations of the cell. Second, the geometry of the cell is entirely defined by level-set functions that are defined independently from the finite element mesh. Simple, regular FEM meshes may, thus, be used regardless of the geometric complexity of the cell. Third, and finally, the different elastic properties and constitutive response of cell cortex are described with a continuum description that naturally fits into the XFEM methodology. Thus, no special treatment is necessary to model jumps in stress, strain and displacement arising due to the cortical membrane.

This paper is organised as follows. In the next section, a description of the cell's deformation is provided and relevant kinematic variables are introduced. In section 3 we then concentrate on deriving the governing equations of surface elasticity and introduce a set of simple elastic constitutive relations for the cytoskeleton and cortical membrane. Numerical considerations are subsequently discussed in Section 4 with the description of an updated Lagrangian XFEM/level-set formulation that is used to investigate the effect of cortex elasticity on the deformation of a contractile cell (Section 5). A summary of the method and concluding remarks are finally provided in Section 6.

2. Kinematics

The first step in deriving the surface elasticity formulation for large deformation is to define consistent measures of deformation. Although the Lagrangian formalism can be used to define total strain measures, many of the complexities associated with mapping mathematical quantities from one material configuration to another can be avoided by using an Eulerian approach. This section, therefore, introduces a rate form of material motion and deformation consistent with the Eulerian framework.

2.1 Generalities

Let us consider a 2D domain Ω in the $x-y$ plane representing a cell Ω_c and its surrounding matrix (Ω_m) such that $\Omega = \Omega_c \cup \Omega_m$ (Figure 1). The interface between the two domains (representing the cell–matrix interface) is denoted as Γ.

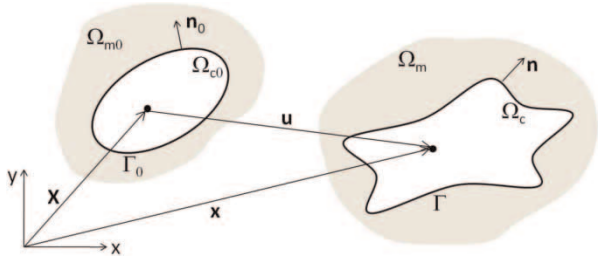

Figure 1. Initial and current configuration of a cell in a 2D plane $x - y$.

In order to introduce the kinematics in the context of large deformations, let us first consider the above domain in two different configurations as shown in the figure. At an initial time $t = t_0$, we represent the medium in the so-called reference configuration (in which the domain and its boundary are represented by Ω_0 and Γ_0, respectively), such that the coordinate of a material point P in a Cartesian coordinate system (x, y) is given by $\mathbf{X} = \{X, Y\}$. A current configuration (in which the domain and its boundary are represented by Ω and Γ, respectively) is then introduced at an arbitrary time t such that the coordinate of the material point P is now given by $\mathbf{x} = \chi(\mathbf{X}, t)$, where χ is assumed to be a smooth function of time and space, except on Γ. Adopting an Eulerian approach, we can relate the bulk deformation of the cell and the matrix to the velocity $\mathbf{v}(\mathbf{x}, t)$ of material point at any time such that

$$\mathbf{v}(\mathbf{x}, t) = \frac{D\mathbf{u}}{Dt}, \quad \text{where } \mathbf{u} = \mathbf{x} - \mathbf{X}, \tag{1}$$

where $\mathbf{u}$ is the displacement and D/Dt denotes the material time derivative that evaluates the variation of a field ($\mathbf{u}$ in the above equation), following a particle P in its motion.

2.2 Deformation measures

In order to accurately describe the deformation of a cell and its surrounding thin cortical membrane, the present work introduces three strain measures that are associated with (a) the deformation of the cell body, (b) the decohesion between the cell and the surrounding matrix and (c) the deformation of the cortical membrane. Following the Eulerian framework, we provide a description of the bulk deformation and rotation of the cell by the rate of deformation tensor $\mathbf{D}(\mathbf{x}, t)$ and the spin $\mathbf{W}(\mathbf{x}, t)$ as follows:

$$\mathbf{D} = \frac{1}{2}(\nabla\mathbf{v} + (\nabla\mathbf{v})^{\mathrm{T}}) \quad \text{and} \quad \mathbf{W} = \frac{1}{2}(\nabla\mathbf{v} - (\nabla\mathbf{v})^{\mathrm{T}}), \tag{2}$$

where ∇ represents the gradient operator with respect to $\mathbf{x}$ and the superscript T is used for the transpose operation. In addition, the present approach allows for a discontinuous velocity field across the cell–matrix interface Γ. As such, a measure of cell–matrix decohesion can simply be introduced through the discontinuity (or jump) $[\mathbf{v}](\mathbf{x}, t)$ in velocity as follows:

$$[\mathbf{v}](\mathbf{x}, t) = \mathbf{v}^{+}(\mathbf{x}, t) - \mathbf{v}^{-}(\mathbf{x}, t), \tag{3}$$

where $\mathbf{x}$ belongs to Γ and $\mathbf{v}^{+}(\mathbf{x})$ and $\mathbf{v}^{-}(\mathbf{x})$ denote velocities on different sides of the interface. Finally, assuming a thin cortical membrane compared to the size of the cell, its deformation may be defined by invoking the concept of surface strain, originally introduced in Gurtin (1998). For this, we introduce a tangential projection operator (in the current configuration) on the cell boundary at point $\mathbf{x}$ as follows:

$$\mathbf{P} = \mathbf{I} - \mathbf{n} \otimes \mathbf{n}, \tag{4}$$

where $\mathbf{I}$ is the second-order identity tensor, while $\mathbf{n} = \mathbf{n}(\mathbf{x}, t)$ is the normal vector to the cell surface in the current configuration. With this definition, the components of the projection of a vector $\mathbf{a}$ and a tensor $\mathbf{A}$ on a surface of normal $\mathbf{n}$ are given by

$$\mathbf{a}_s = \mathbf{P} \cdot \mathbf{a} \quad \text{and} \quad A_s = \mathbf{P} \cdot \mathbf{A} \cdot \mathbf{P}. \tag{5}$$

This geometrical preliminary may now be applied to the definition of the rate of deformation $\mathbf{D}_s$ of the cortical membrane as the tangential projection of the bulk rate of deformation $\mathbf{D}$ onto the cell surface:

$$\mathbf{D}_s = \mathbf{P} \cdot \mathbf{D} \cdot \mathbf{P}. \tag{6}$$

Note that tensor $\mathbf{D}_s$ keeps the same dimension as $\mathbf{D}$ but represents a deformation in space (tangential space) whose dimension is smaller than the original space Ω.

2.3 Evolution equation of the cortical membrane orientation

In general, the cell and matrix geometries are defined in the initial configuration. This means that while the normal vector $\mathbf{n}_0$ and projection operator $\mathbf{P}_0 = \mathbf{I} - \mathbf{n}_0 \otimes \mathbf{n}_0$ are entirely known, their counterparts $\mathbf{n}$ and $\mathbf{P}$ in the current configuration need to be determined. Using the fact that

$$\mathbf{n} = \mathbf{Q} \cdot \mathbf{n}_0 \quad \text{and} \quad \mathbf{P} = \mathbf{Q} \cdot \mathbf{P}_0 \cdot \mathbf{Q}^{\mathrm{T}}, \tag{7}$$

where $\mathbf{Q}$ is the orthonormal transformation (rotation) that maps normal vector from the initial to current configuration. Using the fact that $\mathbf{W} = \dot{\mathbf{Q}}\mathbf{Q}^{\mathrm{T}}$, one can show that

$$\dot{\mathbf{n}} = \mathbf{W} \cdot \mathbf{n} \quad \text{and} \quad \dot{\mathbf{P}} = \mathbf{W}\mathbf{P} + \mathbf{P}\mathbf{W}^{\mathrm{T}}, \tag{8}$$

where a superimposed dot denotes the material time derivative. Equation (8) may thus be integrated in time

in order to determine $\mathbf{n}$ and $\mathbf{P}$ and compute the rate of surface deformation $\mathbf{D}_s$ appearing in (6).

3. Governing equations and constitutive relations

This section concentrates on deriving the equations governing the mechanical equilibrium of a cell undergoing a combination of deformations as introduced above. The equilibrium equations are derived from the energetic considerations, whereas simple elastic relations are given to describe the cell response.

3.1 Principle of virtual power and governing equations

Considering a first-order continuum theory in quasi-static conditions (the kinetic energy of the system is negligible in comparison with deformation and external energies), one can introduce a virtual internal power δP_{int} associated with the medium contained in Ω as follows:

$$\delta P_{\text{int}} = \int_{\Omega} (\mathbf{T} - \mathbf{T}^0) : \delta \mathbf{D}\, \mathrm{d}\Omega + \int_{\Gamma} \left(\mathbf{T}_s - \mathbf{T}_s^0\right) : \delta \mathbf{D}_s \mathrm{d}\Gamma + \int_{\Gamma} \mathbf{T}_d \cdot [\delta \mathbf{v}]\ \mathrm{d}\Gamma, \tag{9}$$

where ':' is the double tensor contraction and $\delta \mathbf{D}$, $\delta \mathbf{D}_s$ and $[\delta \mathbf{v}]$ are small virtual variations of bulk deformation, surface deformation and decohesion around the equilibrium state, respectively. The quantities $\mathbf{T}$, $\mathbf{T}_s$ and $\mathbf{T}_d$ are then defined as power conjugates to the aforementioned deformations and are recognised as the conventional Cauchy stress, surface Cauchy stress and cohesive force, respectively. Furthermore, we also introduced $\mathbf{T}^0$ and $\mathbf{T}_s^0$ as the contractile stresses in the bulk and in the interface, respectively.

Before we write the form of the virtual external power, we make the assumption that the cell is entirely contained in the domain Ω, such that its boundary Γ does not intersect with the domain boundary $\partial\Omega$. This assumption simplifies our analysis as there are no boundary conditions applied on the cell membrane Γ. Furthermore, the domain boundary $\partial\Omega$ is decomposed into two parts according to the nature of the boundary conditions. Introducing as $\partial\Omega_u$ the section of the domain boundary on which a fixed velocity $\bar{\mathbf{v}}$ is applied and as $\partial\Omega_t$ the section of the boundary subjected to a surface traction $\bar{\mathbf{t}}$, the entire boundary can be reconstructed as $\partial\Omega = \partial\Omega_u \cup \partial\Omega_t$. Thus, the external virtual power δP_{ext} finally takes the form:

$$\delta P_{\text{ext}} = \int_{\Omega} \rho \mathbf{b} \cdot \delta \mathbf{v}\, \mathrm{d}\Omega + \int_{\partial\Omega_t} \bar{\mathbf{t}} \cdot \delta \mathbf{v}\, \mathrm{d}\partial\Omega, \tag{10}$$

where ρ is the mass density and $\mathbf{b}$ is a body force per unit mass. We also note that the virtual field $\delta\mathbf{v}$ must vanish on the boundary $\partial\Omega_u$ as required by variational principles (Figure 2). Mechanical equilibrium of the cell and its surrounding matrix is then satisfied upon minimalisation of the total potential energy of the system. In other words, the virtual power

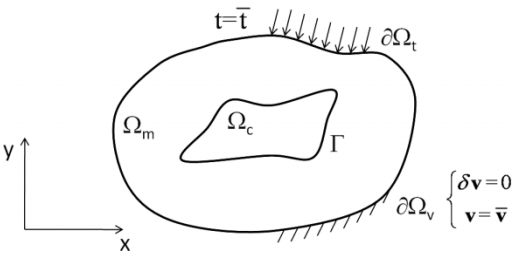

Figure 2. The general outline of a cell along with the surrounding matrix and boundary conditions.

$$\delta P_{\text{int}} - \delta P_{\text{ext}} \tag{11}$$

vanishes for any virtual velocity field in Ω and on Γ. We next use Equation (11) to derive the governing equations (strong form) driving the motion of the cell and its cortical membrane. First, integrating (9) by parts and using the divergence theorem, we can rewrite the virtual internal power as

$$\delta P_{\text{int}} = -\int_{\Omega} (\nabla \cdot \tilde{\mathbf{T}}) \cdot \delta \mathbf{v}\, \mathrm{d}\Omega - \int_{\Gamma} [(\tilde{\mathbf{T}} \cdot \mathbf{n}) \cdot \delta \mathbf{v}]\ \mathrm{d}\Gamma, - \int_{\Gamma} \nabla_s \cdot \tilde{\mathbf{T}}_s \cdot \delta \mathbf{v}^s\, \mathrm{d}\Gamma + \int_{\Gamma} \mathbf{T}_d \cdot [\delta \mathbf{v}]\ \mathrm{d}\Gamma + \int_{\partial\Omega_t} (\tilde{\mathbf{T}} \cdot \mathbf{n}) \cdot \delta \mathbf{v}\, \mathrm{d}\partial\Omega, \tag{12}$$

where $\mathbf{n}$ is the normal unit vector to the surfaces Γ and $\partial\Omega$, $\tilde{\mathbf{T}} = \mathbf{T} - \mathbf{T}^0$ and $\tilde{\mathbf{T}}_s = \mathbf{T}_s - \mathbf{T}_s^0$. Furthermore, we introduced the notation $\nabla_s \cdot \tilde{\mathbf{T}}_s$ to represent the surface divergence of the surface stress $\tilde{\mathbf{T}}_s$. At this point, it is necessary to introduce the average operator $\langle\rangle$ that computes the average of an arbitrary field f on the interface Γ. We write

$$\langle f \rangle = \frac{1}{2}(f^+ + f^-), \tag{13}$$

where f^+ and f^- denote the value of f on opposite sides of the interface. Referring to the work of Gurtin (1998), we can now use the following equalities:

$$[(\tilde{\mathbf{T}} \cdot \mathbf{n}) \cdot \delta \mathbf{v}] = [\tilde{\mathbf{T}} \cdot \mathbf{n}] \cdot \langle \delta \mathbf{v} \rangle + \langle \tilde{\mathbf{T}} \cdot \mathbf{n} \rangle \cdot [\delta \mathbf{v}], \tag{14}$$

$$\nabla_s \tilde{\mathbf{T}}_s \cdot \delta \mathbf{v}_s = \nabla_s \tilde{\mathbf{T}}_s \cdot \langle \delta \mathbf{v} \rangle, \tag{15}$$

together with (12) and (11), to obtain a useful form of the principle of virtual power. For any virtual fields $\delta\mathbf{v}$, $[\delta\mathbf{u}]$

and $\langle \delta \mathbf{u} \rangle$, we have

$$-\int_{\Omega} (\nabla \cdot \tilde{\mathbf{T}} + \rho \mathbf{b}) \cdot \delta \mathbf{v} \, \mathrm{d}\Omega - \int_{\Gamma} ([\tilde{\mathbf{T}} \cdot \mathbf{n}] + \nabla_s \tilde{\mathbf{T}}_s) \cdot \langle \delta \mathbf{v} \rangle \, \mathrm{d}\Gamma$$

$$-\int_{\Gamma} (\langle \tilde{\mathbf{T}} \cdot \mathbf{n} \rangle - \mathbf{T}_d) \cdot [\delta \mathbf{v}] \mathrm{d}\Gamma + \int_{\partial\Omega_t} (\tilde{\mathbf{T}} \cdot \mathbf{n} - \bar{\mathbf{t}}) \cdot \delta \mathbf{v} \, \mathrm{d}\, \partial\Omega = 0. \tag{16}$$

This implies that each integrand appearing in the above expression must vanish for any material point in Ω, Γ and $\partial\Omega_t$. This leads to a system of three coupled differential equations for stresses as follows:

$$\nabla \cdot \tilde{\mathbf{T}} + \rho \mathbf{b} = 0 \quad \text{in } \Omega, \tag{17}$$

$$[\tilde{\mathbf{T}} \cdot \mathbf{n}] + \nabla_s \tilde{\mathbf{T}}_s = 0 \quad \text{on } \Gamma, \tag{18}$$

$$\langle \tilde{\mathbf{T}} \cdot \mathbf{n} \rangle - \mathbf{T}_d = 0 \quad \text{on } \Gamma, \tag{19}$$

subjected to boundary conditions

$$\begin{cases} \tilde{\mathbf{T}} \cdot \mathbf{n} = \bar{\mathbf{t}} & \text{on } \partial\Omega_t \\ \mathbf{v} = \bar{\mathbf{v}} & \text{on } \partial\Omega_v \end{cases} \tag{20}$$

Equations (17)–(19) represent the bulk equilibrium, the balance of forces in the cortical membrane and the balance of cohesive forces between a cell and the ECM, respectively.

3.2 Constitutive relation

For the sake of simplicity, we now introduce a set of simple elastic constitutive relations for the cytoskeleton and the cortical membrane. Although the present analysis is general enough to consider more realistic nonlinear material responses, the present work concentrates on linear elastic relations between stress and strain. The Eulerian framework described here requires that constitutive relations are given in a rate form, i.e. it is written in terms of a material time derivative of the Cauchy stress and rates of deformation. However, to ensure that elastic energy is conserved during deformation, it is important to describe the elastic response of the cytoskeleton in terms of a hyper-elastic potential Ψ, that is a function of the deformation gradient $\mathbf{F} = \nabla_{\mathbf{X}} \mathbf{x}$, where $\nabla_{\mathbf{X}}$ is the gradient operator in the reference configuration. A common model used for isotropic elastic materials is provided by the neo-Hookean model, for which the strain energy function Ψ is expressed in terms of the Lame constants λ and μ as follows:

$$\rho_0 \Psi = \frac{1}{2}\lambda (\ln J)^2 - \mu \ln J + \frac{1}{2}\mu (I_1 - 3), \tag{21}$$

where ρ_0 is the mass density of the cytoplasm in the reference configuration and the strain invariants I_1 and J are given by $I_1 = \mathrm{trace}(\mathbf{F}^{\mathrm{T}}\mathbf{F})$ and $J = \det(\mathbf{F})$. Following (Belytschko et al. 2000), we can show that the above model implies that an objective stress rate $\mathbf{T}^{\sigma J}$ (more specifically the Jaumann rate) can be written in terms of the rate of deformation $\mathbf{D}$ introduced in (2) as follows:

$$\mathbf{T}^{\sigma J} = \mathbf{C}^{\sigma J} : \mathbf{D}, \tag{22}$$

where the components of the fourth-order elastic matrix $\mathbf{C}^{\sigma J}$ take the form

$$C^{\sigma J}_{ijkl} = 2(\mu - \lambda \ln J)\delta_{ik}\delta_{jl} + \lambda \delta_{ij}\delta_{kl}. \tag{23}$$

In the above equation, δ is the Dirac delta function. Let us now introduce the elastic response of the cortical membrane. Concentrating on plane stress problems, we may view the membrane surrounding the cell as a 1D cable undergoing axial deformation ε. As a result, the cortical stiffness may be defined in terms of a scalar quantity denoted as K_s, such that the rate of elastic energy P^s corresponding to an axial strain rate $\dot{\varepsilon}$ is written as follows:

$$P^s = \frac{1}{2} K_s \dot{\varepsilon}^2 = \frac{1}{2} K_s \mathbf{D}_s : \mathbf{D}_s, \tag{24}$$

where we used the fact that $\mathbf{D}_s : \mathbf{D}_s = \dot{\varepsilon}^2$. An objective rate of surface stress $\mathbf{T}^{s,\sigma J}$ may, thus, be defined as the derivative of P^s with respect to the rate of deformation $\mathbf{D}_s$ as

$$\mathbf{T}^{s,\sigma J} = \frac{\partial^2 \Psi^s}{\partial \mathbf{D}_s \ \partial \mathbf{D}_s} : \mathbf{D}_s = \mathbf{S}_s : \mathbf{D}_s, \tag{25}$$

where the components $S_{s,ijkl}$ of the cortical membrane elastic tensor are written in terms of the cortex stiffness K_s as follows:

$$S_{s,ijkl} = K_s \ \ \delta_{ik} \ \ \delta_{jl}. \tag{26}$$

Finally, this study concentrates on the case of 'free cells' that are not interacting with an ECM. The surrounding matrix material is, therefore, not considered, and thus, no cohesive forces are present. This means that $\mathbf{T}^d = \mathbf{0}$ throughout this study. To complete the form of the constitutive framework, it is now of interest to relate the material time derivative of stresses (that is not an objective measure) to the Jaumann stress rate introduced above. Following (Belytschko et al. 2000), we write

$$\dot{\mathbf{T}} = \frac{D\mathbf{T}}{Dt} = \mathbf{T}^{\sigma J} + \mathbf{W} \cdot \mathbf{T} + \mathbf{T} \cdot \mathbf{W}^{\mathrm{T}}, \tag{27}$$

where $\mathbf{W}$ is the spin tensor defined in (2). It can be shown that the above equation is true for both bulk and surface

stress and, thus, can be used to compute rates of $\mathbf{T}_s$, $\mathbf{T}_s^0$ and $\mathbf{T}^0$ appearing in this study.

4. Numerical solution: an XFEM strategy

This section provides a numerical strategy to solve governing Equations (17)–(19), together with constitutive relations (25) and (22). A particularity of these equations is that they give rise to discontinuities in strain rate and velocities across the cell's interface, a feature that cannot be naturally handled with linear finite elements. The XFEM formalism (Dolbow et al. 2001; Belytschko et al. 2003) is, therefore, utilised to overcome this issue.

4.1 Extended XFEM

The XFEM equations are developed within the so-called updated Lagrangian method (for more information on this method, the reader is referred to Belytschko et al. (2000), by using the final weak form derived in (16). The solution of these equations typically gives rise to discontinuities across the interface Γ. Indeed, the existence of surface tension is associated with a jump in strain across the interface (commonly called weak discontinuity), whereas the existence of a decohesion (through the cohesive law) leads to a jump in displacement across Γ (commonly called strong discontinuity). Many numerical techniques, such as the FEM, are developed for continuous fields and, therefore, fail to describe such discontinuities. To address this issue, the XFEM was first introduced to incorporate a jump in displacement occurring as a result of a propagating crack in a continuous medium (Dolbow et al. 2001; Hettich et al. 2008). A key feature of this method is that the description of the discontinuity is independent of spatial discretisation. Thus, Belytschko et al. used XFEM in Belytschko et al. (2003) and Belytschko and Gracie (2007) to define solids by implicit surfaces and also to model dislocations and interfaces. The method was further improved to model weak discontinuities, such as that described in Moes et al. (2003). This method provides a natural platform on which (16) can be solved with great flexibility and minimal computation cost. In the present formulation, domain Ω is first subdivided into four-node quadrilateral elements in which an approximation $\tilde{\mathbf{v}}(\mathbf{x})$ of the velocity field is sought. To account for the existence of continuous, strong and weak discontinuous fields within an element, we write $\tilde{\mathbf{v}}(\mathbf{x})$ as the sum of three terms that are parametrised by $\mathbf{v}$, $\bar{\mathbf{v}}$ and $\bar{\bar{\mathbf{v}}}$ as follows:

$$\tilde{\mathbf{v}}^e(\mathbf{x}) = \sum_{I=1}^{n} \mathbf{N}_I(\mathbf{x})\mathbf{v}_I + \sum_{J=1}^{m} \mathbf{N}_J(\mathbf{x})(H(\mathbf{x}) - H(\mathbf{x}_J))\bar{\mathbf{v}}_J + \sum_{J=1}^{m} \mathbf{N}_J(\mathbf{x})\chi_J(\mathbf{x})\bar{\bar{\mathbf{v}}}_J, \tag{28}$$

where

$$\mathbf{N}_I(\mathbf{x}) = \begin{bmatrix} N_I(x) & 0 \\ 0 & N_I(x) \end{bmatrix}. \tag{29}$$

Functions $N_I(\mathbf{x})$ are finite element shape functions associated with node, $I, N_J(\mathbf{x})$ are the shape functions associated with the nodes of an element that has been cut by the interface (see Figure 3) and n is the total number of nodes per element, whereas m is the number of enriched nodes ($m \leq n$). Furthermore, the quantities $H(\mathbf{x})$ and $\chi(\mathbf{x})$ are enrichment functions with the required discontinuities (Heaviside function and ridge function, respectively (Moes et al. 2003; Mohammadi 2008)). Referring to Figure 3(c),(d), the Heaviside function introduces a jump in velocity (strong discontinuity), in contrast, a ridge function causes a jump in the spatial derivative of the velocity (weak discontinuity) across the interface. In 1D, the Heaviside and ridge functions take the form

$$H(\phi) = \begin{cases} 1 & \phi > 0 \\ 0 & \phi < 0 \end{cases} \quad \text{and} \quad \chi_j(\mathbf{x}) = |\phi(\mathbf{x})| - |\phi(\mathbf{x}_j)|. \tag{30}$$

To define the geometry of a cell in the reference configuration (defined by Ω_0 and Γ_0), we introduce

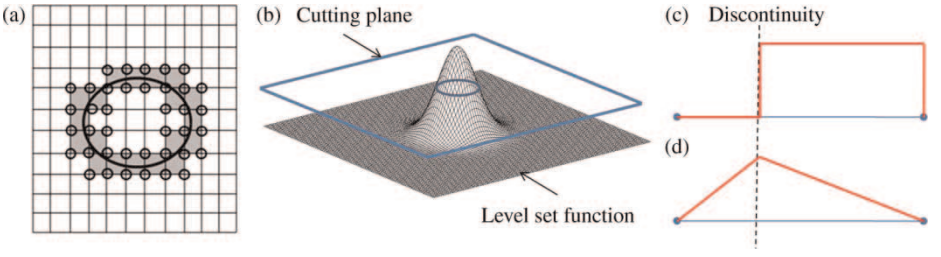

Figure 3. (a) Enriched nodes and completely enriched elements for a closed interface. (b) Level-set function and cutting plane to define a circular cell in a square domain. (c) A typical Heaviside (step) function to define strong discontinuity and (d) A typical ridge function to define weak discontinuity.

a level-set function $\phi(\mathbf{X})$ such that the interface (or cell boundary) is defined as the intersection of a level-set surface with a cutting plane, as depicted in Figure 3(b). With this description, the sign of ϕ is opposite in two sides of the discontinuity. An attractive feature of using a levelset formulation is that initial unit vectors $\mathbf{n}_0$ that are normal to the interface are determined by the gradient of the function $\phi(\mathbf{X})$ with respect to the initial coordinates $\mathbf{X}$ as follows (Figure 1):

$$\mathbf{n}_0(x) = \frac{\nabla_{\mathbf{X}}\phi(x)}{\|\nabla_{\mathbf{X}}\phi(x)\|}. \tag{31}$$

Using this definition and evolution Equation (8), the projection operator $\mathbf{P}$ in the current configuration may be obtained by time integration.

4.2 Linearised XFEM equations

To derive a finite element form of the governing equation, we first associate each node of an element with velocity degrees of freedom $\mathbf{v}^e$ that comprise contributions from three terms introduced in (28):

$$\mathbf{v}^e = \begin{bmatrix} \mathbf{v} & \bar{\mathbf{v}} & \bar{\bar{\mathbf{v}}} \end{bmatrix}^{\mathrm{T}}. \tag{32}$$

Note that the full set of degrees of freedom only appear when an element intersects with the cell boundary. Using the XFEM approximation (28), we write the rates of deformation $\{\mathbf{D}^e\}$ and $\{\mathbf{D}^e_s\}$ within an element in Voigt notation as

$$\{\mathbf{D}^e\} = \begin{bmatrix} D^e_{11} \\ D^e_{22} \\ 2D^e_{12} \end{bmatrix} = \mathbf{B}\cdot\mathbf{v}^e \text{ and } \left\{\mathbf{D}^e_s\right\} = \begin{bmatrix} D^e_{s11} \\ D^e_{s22} \\ 2D^e_{s12} \end{bmatrix} = \mathbf{M}_p\cdot\{\mathbf{D}^e\}, \tag{33}$$

where the $\mathbf{B}$ matrix relates nodal velocities and rate of deformation and takes the form

$$\mathbf{B} = \begin{bmatrix} \mathbf{B}_1 & \mathbf{B}_2 & \dots & \mathbf{B}_{n+m} \end{bmatrix} \text{ and } \mathbf{B}_I = \begin{bmatrix} \frac{\partial \bar{N}_I(\mathbf{x})}{\partial x_1} & 0 \\ 0 & \frac{\partial \bar{N}_I(\mathbf{x})}{\partial x_2} \\ \frac{\partial \bar{N}_I(\mathbf{x})}{\partial x_2} & \frac{\partial \bar{N}_I(\mathbf{x})}{\partial x_1} \end{bmatrix}, \tag{34}$$

while the matrix $\mathbf{M}_p$ represents the tangential projection (in Voigt notation) of the bulk quantity $\mathbf{D}$ to obtain the rate of surface deformation $\mathbf{D}_s$ as shown in (6). It can be shown (Yvonnet et al. 2008) that $\mathbf{M}_p$ can be written as

$$\mathbf{M}_p = \begin{bmatrix} P^2_{11} & P^2_{12} & P_{11}P_{12} \\ P^2_{12} & P^2_{22} & P_{22}P_{12} \\ 2P_{11}P_{12} & 2P_{22}P_{12} & P^2_{12} + P_{11}P_{22} \end{bmatrix}, \tag{35}$$

where P_{ij} are the components of the projection tensor $\mathbf{P}$ introduced in (4). To obtain a discretised weak form of the governing equation, let us first consider the virtual powers considered in (9) and (10) and then decompose the integration over the entire domain Ω into a sum of integration over element domains Ω_e. Furthermore, using the XFEM interpolation (33), one can show that numerical approximations $\delta\tilde{P}_{\text{int}}$ and $\delta\tilde{P}_{\text{ext}}$ of virtual powers (9) and (10) can be written as follows:

$$\begin{aligned} \delta\tilde{P}_{\text{int}} =& \sum_e \left\{ \int_{\Omega^e} \{\delta\mathbf{D}^e\}^{\mathrm{T}}\cdot\{\mathbf{T}\}\mathrm{d}\Omega + \int_{\Gamma} \left\{\delta\mathbf{D}^e_s\right\}^{\mathrm{T}}\cdot\{\mathbf{T}_s\}\mathrm{d}\Gamma \right. \\ & \left. - \int_{\Omega^e} \{\delta\mathbf{D}^e\}^{\mathrm{T}}\cdot\{\mathbf{T}^0\}\mathrm{d}\Omega - \int_{\Gamma_e} \left\{\delta\mathbf{D}^e_s\right\}^{\mathrm{T}}\cdot\left\{\mathbf{T}^0_s\right\}\mathrm{d}\Gamma_e \right\} \\ \delta\tilde{P}_{\text{ext}} =& \sum_e \left\{ \int_{\Omega_e} \rho\delta(\mathbf{v}^e)^{\mathrm{T}}\cdot\mathbf{b}\,\mathrm{d}\Omega + \int_{\partial\Omega_{te}} \delta(\mathbf{v}^e)^{\mathrm{T}}\cdot\bar{\mathbf{t}}\,\mathrm{d}\partial\Omega_{te} \right\}, \end{aligned} \tag{36}$$

where stress measures are written in Voigt notation in the form $\{\mathbf{T}\} = [T_{11}\ T_{22}\ T_{12}]^{\mathrm{T}}$. Moreover, because we assumed that there is no cohesion between cell and its surrounding matrix, the above equation is true for a vanishing cohesive term $\mathbf{T}_d = 0$. To derive a numerical solution of the nonlinear governing equations, it is now necessary to linearise the above expressions. For this, we linearise stresses following $\{\mathbf{T}\} = \{\mathbf{T}\} + \{\dot{\mathbf{T}}\}\delta t$, where δt is a small time increment. Following expressions (27) for the material time derivative of Cauchy stresses, the spin dependence of the objective stress rate takes the form:

$$\{\mathbf{W}\cdot\mathbf{T} + \mathbf{T}\cdot\mathbf{W}^{\mathrm{T}}\} = \mathbf{T}^v W = \mathbf{T}^v(\mathbf{G}\cdot\dot{\mathbf{d}}^e), \tag{37}$$

where

$$\mathbf{T}^v = [2T_{12} - 2T_{12}T_{22} - T_{11}]^{\mathrm{T}},$$

and

$$\mathbf{G} = \begin{bmatrix} \mathbf{G}_1\mathbf{G}_2\dots\mathbf{G}_{m+n} \end{bmatrix} \quad \text{and } \mathbf{G}_I = 0.5\left[\frac{\partial\bar{\mathbf{N}}_I(\mathbf{x})}{\partial x_2} - \frac{\partial\bar{\mathbf{N}}_I(\mathbf{x})}{\partial x_1}\right]. \tag{38}$$

Equation (37) can also be written for surface and contractile stresses $\mathbf{T}_s$, $\mathbf{T}^0$ and $\mathbf{T}^0_s$, respectively. Finally, using constitutive relations (22) and (25), linearised

versions of the virtual powers read

$$\begin{aligned}\delta\tilde{P}_{\text{int}} = \sum_e \Bigg(& \int_{\Omega^e} (\mathbf{B}\cdot\delta\mathbf{v}^e)^{\mathrm{T}}(\{\mathbf{T}\}+\{\mathbf{C}\}\cdot(\mathbf{B}\cdot\mathbf{v}^e)\cdot\delta t \\ & +\mathbf{T}^v(\mathbf{G}\cdot\mathbf{v}^e)\cdot\delta t)\mathrm{d}\Omega^e \\ & +\int_{\Gamma^e} (\mathbf{M}_p\cdot\mathbf{B}\cdot\delta\mathbf{v}^e)^{\mathrm{T}}(\{\mathbf{T}^s\}+\{\mathbf{C}_s\}\cdot(\mathbf{M}_p\cdot\mathbf{B}\cdot\mathbf{v}^e)\cdot\delta t \\ & +\mathbf{T}_s^v(\mathbf{G}\cdot\mathbf{v}^e)\cdot\delta t)\mathrm{d}\Gamma^e \\ & -\int_{\Omega^e} (\mathbf{B}\cdot\delta\mathbf{v}^e)^{\mathrm{T}}\cdot(\{\mathbf{T}^0\}+\{\mathbf{T}^0\}^{\sigma J}\cdot\delta t \\ & +\mathbf{T}^{0,v}(\mathbf{G}\cdot\mathbf{v}^e)\cdot\delta t)\mathrm{d}\Omega^e \\ & -\int_{\Gamma^e} (\mathbf{M}_p\cdot\mathbf{B}\cdot\delta\mathbf{v}^e)^{\mathrm{T}}\cdot\Big(\{\mathbf{T}_s^0\}+\{\mathbf{T}_s^0\}^{\sigma J}\cdot\delta t \\ & +\mathbf{T}_s^{0,v}(\mathbf{G}\cdot\mathbf{v}^e)\cdot\delta t\Big)\mathrm{d}\Gamma^e\Bigg),\end{aligned} \tag{39}$$

$$\delta\tilde{P}_{\text{ext}} = \sum_e \left(\int_{\Omega^e} \rho(\mathbf{N}\cdot\delta\mathbf{v}^e)^{\mathrm{T}}\cdot\mathbf{b}\,\mathrm{d}\Omega^e + \int_{\partial\Omega_t^e} (\mathbf{N}\cdot\delta\mathbf{v}^e)^{\mathrm{T}}\cdot\bar{\mathbf{t}}\,\mathrm{d}\partial\Omega_t^e \right). \tag{40}$$

In the above equation, the second-order matrices $\{\mathbf{C}\}$ and $\{\mathbf{C}_s\}$ are the cytoskeleton and the cortical membrane elastic matrices in Voigt notation, respectively (note that we deleted the superscript 'σJ' and 'e' to lighten the expression). In addition, the relationship between the stiffness matrix $\{\mathbf{C}_s\}$ of cortical membrane and its elasticity matrix $\{\mathbf{S}\}^s$ was taken as

$$\{\mathbf{C}_s\} = \mathbf{M}_p^T\{\mathbf{S}\}^s\mathbf{M}_p, \tag{41}$$

where $\mathbf{M}_p$ is defined in (35). After factorising and simplifying the above expressions, one can derive a more convenient form of the virtual powers as follows:

$$\begin{aligned}\delta\tilde{P}_{\text{int}} = \sum_e \delta\mathbf{v}^{eT}\Bigg(& \int_{\Omega^e} \mathbf{B}^{\mathrm{T}}(\{\mathbf{T}\}+\{\mathbf{C}\}\cdot(\mathbf{B}\cdot\delta\mathbf{v}^e) \\ & +\mathbf{T}^v(\mathbf{G}\cdot\delta\mathbf{v}^e))\mathrm{d}\Omega^e \\ & +\int_{\Gamma^e} \mathbf{B}^{\mathrm{T}}\cdot\mathbf{M}_p^T\big(\{\mathbf{T}^s\}+\{\mathbf{C}_s\}\cdot(\mathbf{M}_p\cdot\mathbf{B}\cdot\delta\mathbf{v}^e) \\ & +\mathbf{T}_s^v(\mathbf{G}\cdot\delta\mathbf{v}^e)\big)\mathrm{d}\Gamma^e \\ & -\int_{\Omega^e} \mathbf{B}^{\mathrm{T}}\cdot(\{\mathbf{T}^0\}+\{\delta\mathbf{T}^0\}+\mathbf{T}^{0,v}(\mathbf{G}\cdot\delta\mathbf{v}^e))\mathrm{d}\Omega^e \\ & -\int_{\Gamma^e} \mathbf{B}^{\mathrm{T}}\cdot\mathbf{M}_p^T\cdot\big(\{\mathbf{T}_s^0\}+\{\delta\mathbf{T}_s^0\}+\mathbf{T}_s^{0,v}(\mathbf{G}\cdot\delta\mathbf{v}^e)\big)\mathrm{d}\Gamma^e\Bigg),\end{aligned} \tag{42}$$

$$\delta\tilde{P}_{\text{ext}} = \sum_e \delta\mathbf{v}^{eT}\left(\int_{\Omega^e} \rho\,\mathbf{N}^{\mathrm{T}}\cdot\mathbf{b}\,\mathrm{d}\Omega^e + \int_{\partial\Omega_t^e} \mathbf{N}^{\mathrm{T}}\cdot\bar{\mathbf{t}}\,\mathrm{d}\partial\Omega_t^e \right). \tag{43}$$

Finally, using the principle of virtual power (11) and substituting the approximations of the virtual powers (42) and (43), we obtain the following finite element equation:

$$\sum_e \big(\mathbf{K}_{\text{int}}^e\big)\cdot\delta\,\mathbf{d} = \sum_e \big(\mathbf{F}_{\text{ext}}^e - \mathbf{F}_{\text{int}}^e\big), \tag{44}$$

where $\mathbf{K}_{\text{int}}^e$ denotes the internal stiffness of element e and takes the form

$$\begin{aligned}\mathbf{K}_{\text{int}}^e = & \int_{\Omega^e} \mathbf{B}^{\mathrm{T}}\cdot\{\mathbf{C}\}\cdot\mathbf{B} + \mathbf{B}^{\mathrm{T}}\cdot\mathbf{T}^v\cdot\mathbf{G}\,\mathrm{d}\Omega^e \\ & + \int_{\Gamma^e} \mathbf{B}^{\mathrm{T}}\cdot\mathbf{M}_p^T\cdot\{\mathbf{C}_s\}\cdot\mathbf{M}_p\cdot\mathbf{B} \\ & + \mathbf{B}^{\mathrm{T}}\cdot\mathbf{M}_p^T\cdot\mathbf{T}_s^v\cdot\mathbf{G}\,\mathrm{d}\Gamma^e \\ & - \int_{\Omega^e} \mathbf{B}^{\mathrm{T}}\cdot\mathbf{T}^{0,v}\cdot\mathbf{G}\,\mathrm{d}\Omega^e \\ & - \int_{\Gamma^e} \mathbf{B}^{\mathrm{T}}\cdot\mathbf{M}_p^T\cdot\mathbf{T}_s^{0,v}\cdot\mathbf{G}\,\mathrm{d}\Gamma^e,\end{aligned} \tag{45}$$

while the internal and external forces associated with element e are written as follows:

$$\begin{aligned}\mathbf{F}_{\text{int}}^e = & \int_{\Omega^e} \mathbf{B}^{\mathrm{T}}\cdot\{\mathbf{T}\}\mathrm{d}\Omega^e + \int_{\Gamma^e} \mathbf{B}^{\mathrm{T}}\cdot\mathbf{M}_p^T\cdot\{\mathbf{T}^s\}\mathrm{d}\Gamma^e \\ & - \int_{\Omega^e} \mathbf{B}^{\mathrm{T}}\cdot\{\mathbf{T}^0\}\mathrm{d}\Omega^e \\ & - \int_{\Gamma^e} \mathbf{B}^{\mathrm{T}}\cdot\mathbf{M}_p^T\cdot\big\{\mathbf{T}_s^0\big\}\mathrm{d}\Gamma^e,\end{aligned} \tag{46}$$

$$\mathbf{F}_{\text{ext}}^e = \int_{\Omega^e} \rho\,\mathbf{N}^{\mathrm{T}}\cdot\mathbf{b}\,\mathrm{d}\Omega^e + \int_{\partial\Omega_t^e} \mathbf{N}^{\mathrm{T}}\cdot\bar{\mathbf{t}}\,\mathrm{d}\partial\Omega_t^e. \tag{47}$$

The quantities are then numerically evaluated using Gaussian quadrature for which four integration points are considered in normal and partially enriched elements. However, integration in fully enriched elements is carried out by subdividing elements into sub-triangles following (Dolbow 1999), and integration on the cell surface follows from the assumption that the interface is straight within an element (this only requires two integration points on the interface). The reader is referred to Farsad et al. (2010) for a more complete description of the integration scheme used in this study. The finite element Equation (44) has been implemented in a Fortran computer program following the flow chart presented in Figure 4. To summarise, a solution $\mathbf{d}$ of the nodal displacements is obtained as a function of time by computing a solution of (44) at different time increments Δt and proceeding to time integration of various quantities such as velocities and the projection operator. At each time increment, the determination of incremental displacements $\Delta\mathbf{d}$ follows

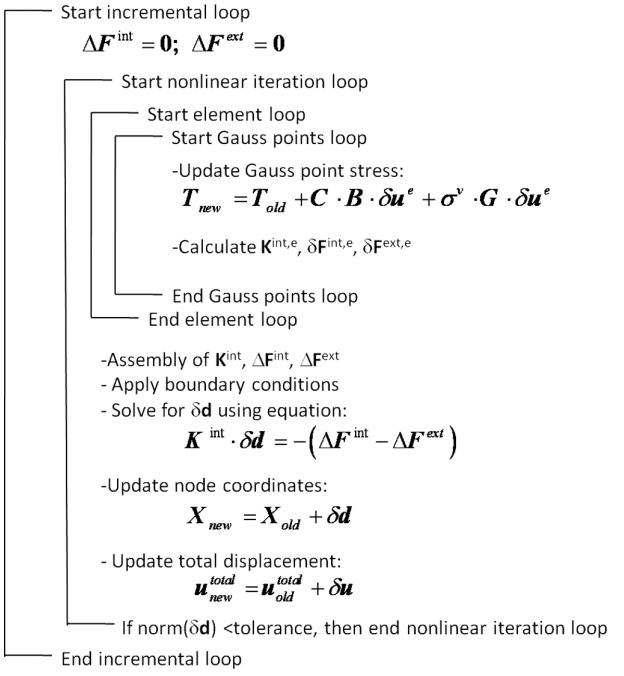

Figure 4. The updated Lagrangian algorithm used in the nonlinear solution of the XFEM equations to determine cell deformation.

from an iterative Newton–Raphson procedure such that $\Delta\mathbf{d} = \sum_{\text{nitr}} \delta\mathbf{d}$, where vector $\delta\mathbf{d}$ denotes the nodal displacements of each iteration and nitr stands for the number of nonlinear iterations. After each iteration, stresses, coordinates and normal vectors are updated using general evolution Equations (27) and (8). Finally, the total nodal displacements are calculated by $\mathbf{d} = \sum_{\text{ninc}} \Delta\mathbf{d}$, where ninc stands for the number of increments.

A significant advantage in using the above formulation is that the complex shapes of cells (Figure 2) are described with a level-set function independently of finite element discretisation. Issues related to meshing complex shapes (in two and three dimensions) are, therefore, totally alleviated. Another important remark is that while, in general, cell motion depends on the deformation of the external matrix due to cell-matrix cohesion, the lack of a cohesive stress $\mathbf{T}_d$ precludes these interactions. As a result, cell and matrix may be considered as two independent bodies undergoing independent deformations. Since the two bodies are originally defined as connected domains on a single finite element mesh, the capability of XFEM to describe discontinuities in velocities between the two domains is critical.

5. Numerical investigation of the role of the cortical membrane on cell deformation

The objective of this section is to validate the model and provide a general analysis of the role of the cortical membrane on cell deformation using the proposed model. For the sake of simplicity, this study concentrates on an initially square cell whose displacements are constrained at its four corners in order to mimic adhesion to a stiff substrate (Figure 5(a)). Furthermore, the cell is described by material properties shown in Table 1 and following (Deshpande et al. 2006), we subjected the cytoskeleton to an isotropic contractile stress $\mathbf{T}^0 = T^0\mathbf{I}$ generated by randomly oriented stress fibres in the cytoskeleton. On the computational side, domain Ω was discretised into a 19*19 regular finite element square mesh of total size 50 μm. The cell domain Ω_c was defined by a level-set function representing a square domain spanning about 15 elements, for which the four corner elements were subjected to a constrained displacement. We have shown that this choice of discretisation gave a good combination of efficiency and convergence.

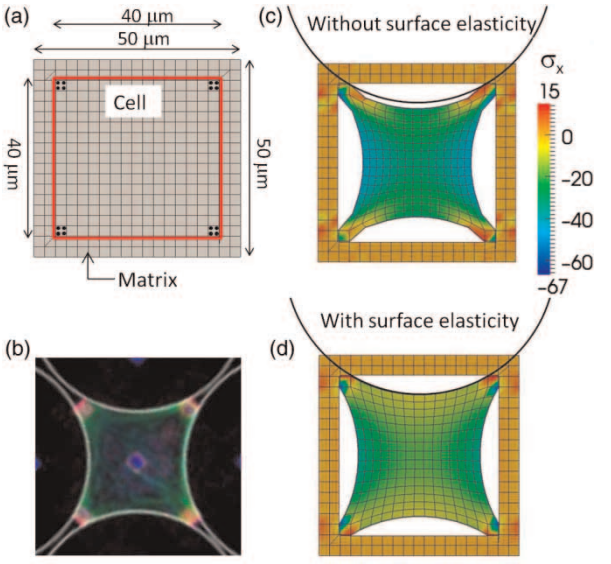

Figure 5. (a) Initial configuration, (b) deformed configuration of a cell on adhesion islands Bischofs et al. (2008), (c) deformed configurations of a square cell without and (d) with cortical membrane.

5.1 Effect of cortical stiffness on cell deformation

The first example consists in investigating the general effect of the cortical membrane on cell deformation. The deformed configuration of the cell is then studied in two

Table 1. Physical constants used in simulations.

Constant	Value	Reference
E	77 Pa	Deshpande et al. (2006)
ν	0.3	Deshpande et al. (2006)
K_s	0.1 N/m	
T_s^0	0 N/m	
T^0	45 Pa	Deshpande et al. (2006)

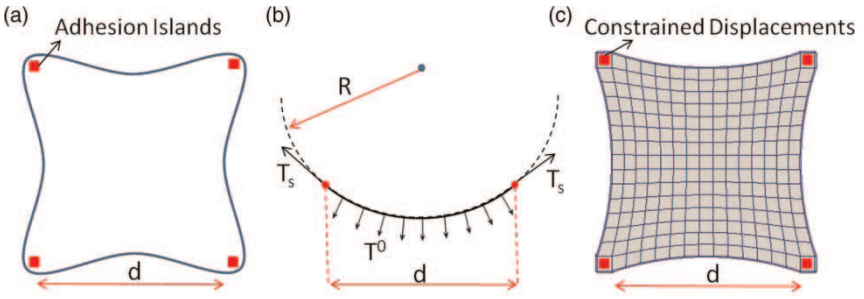

Figure 6. The models used in the analytical and numerical solutions. (a) the deformed configuration of the cell to be modelled, (b) the analytical model and (c) the numerical model.

cases: (a) no cortical stiffness and (b) the cortical stiffness given by $K_s = 0.1\,N/m$.

As shown in Figure 5, the presence of a cortical membrane (when $K_s = 0.1\,N/m$) results in the homogenisation of surface strains and surface curvatures. This is not surprising as cortical stiffness acts against surface deformation. A consequence of this is that the cell boundary is characterised by a circular shape between two adhesion regions, a result that is confirmed by the experimental work of Bischofs et al. (2008) on fibroblasts (Figure 5(b)). Furthermore, upon observing the stress distribution in the cytoskeleton in Figure 5, one sees that a cell without cortical membrane is subjected to a large stress concentration near its corner, whereas internal stresses are more uniform when cortical stiffness increases. This suggests a possible role of the cortical membrane in protecting the cell against large stresses and possible damage, especially in adhesion regions that are prone to undergo large variations of both surface and bulk deformations.

5.2 *Relationship between cortical stiffness and membrane curvature*

Let us now investigate how membrane curvature varies in terms of cortical stiffness K_s and contractile stress T^0. In particular, it is of interest to compare the numerical solution derived in this paper to the analytical solution of a cable, attached at its two ends and subjected to a distributed external force T^0 acting perpendicular to the cable's direction (Figure 6(b)). If we consider the external force as the cytoskeleton's contractile stress, then this problem provides a benchmark with which our numerical solution can be compared, when cytoskeleton elasticity becomes negligible compared with cortical stiffness.

Considering that the spanning distance, d, does not change during deformation and that the cortex has constant curvature with line tension T_s and stiffness K_s, one can show that the radius of curvature, R, of the membrane is (Bischofs et al. 2008)

$$R = \frac{T_s}{T^0} = \frac{K_s}{T^0}\left(\frac{L-\alpha d}{\alpha d}\right), \tag{48}$$

where $L = 2R\arcsin(d/2R)$ and αd are the current and reference length of the arc, respectively. Rearranging the equations finally leads to the following relationship between the cortex curvature κ, the cortical stiffness K_s and the contractile stress T^0:

$$\frac{1}{\kappa d} = \frac{K_s}{T^0 d}\left(\frac{2}{\alpha\kappa d}\arcsin\left(\frac{\kappa d}{2}\right) - 1\right). \tag{49}$$

To compare analytical and numerical prediction, we then studied the relationship between the non-dimensional surface curvature κd and the ratio $K^s/T^0 d$ of cortical stiffness and contractile stress as depicted in Figure 7. Results show a net decrease in membrane curvature with increasing cortical stiffness, with noticeable differences between the analytical and numerical predictions for small values of $K^s/T^0 d$. These trends may be explained as follows. For large values of $K^s/T^0 d$, the stiffness of the cortical membrane is significantly higher than the stiffness of the bulk cytoskeleton, and the assumptions of the analytical model are acceptable. As a consequence, numerical and analytical predictions coincide. However, for small values of $K^s/T^0 d$, the effect of the bulk cytoskeleton has a large influence on cell deformation, a feature that is not predicted by the analytical model. In this case, bulk stiffness provides a resistance to membrane

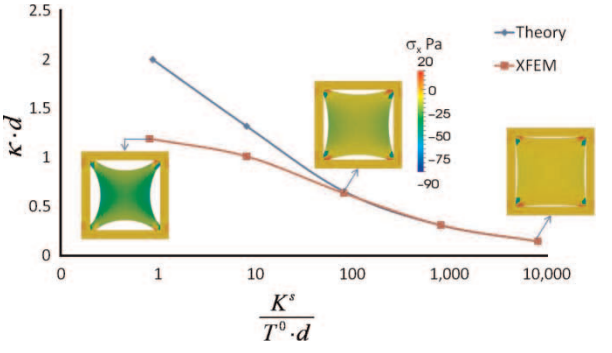

Figure 7. Effect of normalised cortex's stiffness on normalised membrane curvature predicted by the numerical (XFEM) and theoretical solutions.

curvature by limiting the deformation of the internal cytoskeleton. These results show significantly smaller surface curvature than those of analytical prediction. These results are important for two reasons: (a) they validate the proposed numerical method to study the effect of the membrane cortex on cell deformation in the region of large cortical stiffness and (b) they extend the range of prediction provided by the analytical solution by incorporating the role of cytoskeleton elasticity on membrane curvature.

5.3 *Relative influence of cytoskeleton and cortical membrane on cell contraction*

Next, we propose to investigate the effects of three intrinsic cell properties (cytoskeleton's Young's modulus E, cytoskeleton's Poisson's ratio ν and cortical tension T_s^0) on the curvature of the cortical membrane. Such knowledge is potentially relevant in understanding how cells can modify their shape by adjusting the properties of their cytoskeleton.

5.3.1 *Young's modulus*

In this example, the Eulerian XFEM formulation is used to assess the effect of cytoskeleton's Young's modulus on the cell membrane curvature after deformation. For this, we considered a cell whose properties are given in Table 1 and for which Young's modulus is varied from 77 to 150 Pa. Results are summarised in Figure 8.

The results show how an increase in cytoskeleton's Young's modulus tends to decrease membrane curvature. This effect is particularly noticeable for small values of cortical stiffness. These results, therefore, emphasise the fact that the role of the cortical membrane on cell's deformation is increasingly important and cannot be neglected, as cytoskeleton stiffness decreases.

5.3.2 *Poisson's ratio*

Another material parameter of interest is Poisson's ratio of the cytoskeleton. The next investigation, therefore, consisted in varying the value of ν from 0 to 0.5 (for which the cytoskeleton becomes an incompressible material), while keeping the other material parameters constant and equal to those presented in Table 1. Figure 9 shows the changes of cortex curvature with cortex stiffness ($K_s/T^0 d$) as the Poisson's ratio of the cytoskeleton is varied.

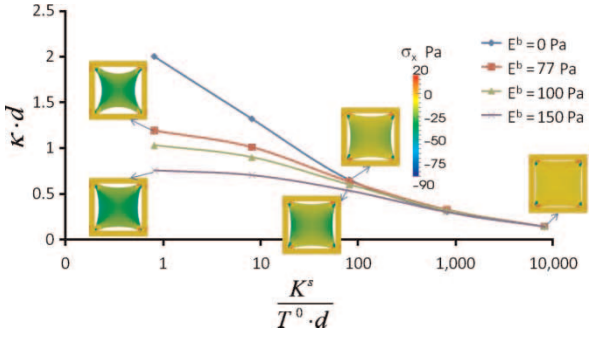

Figure 8. Effect of the cytoskeleton's Young's modulus on the normalised curvature of the cortical membrane.

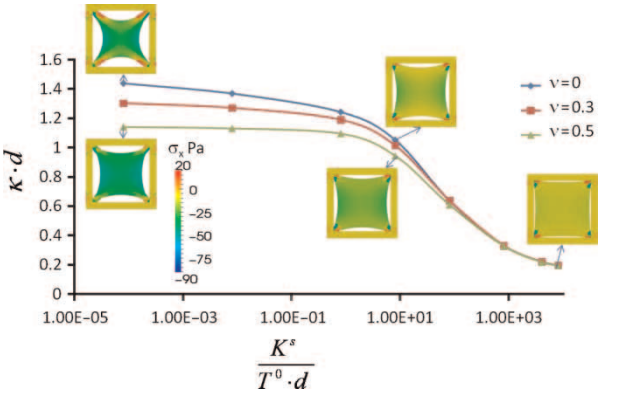

Figure 9. Effect of cytoskeleton's Poisson's ratio on the normalised curvature of cortical membrane.

General trends show that increasing Poisson's ratio results in increasing the resistance of the cytoskeleton and, therefore, decreasing membrane curvatures. Moreover, it is observed that for high Poisson's ratio (close to 0.5), the curvature becomes independent of the surface stiffness for small values of the cortical stiffness. This may be explained by the fact that for high Poisson's ratios, the cytoskeleton becomes nearly incompressible and shear deformation is favoured over volume changes. Cytoskeleton stress is thus modified near the membrane, limiting the magnitude of tangential stretch and homogenising membrane curvature, even for relatively low membrane stiffness. Furthermore, it is interesting to note that even for an incompressible cytoskeleton ($\nu \approx 0.5$), we observe a change in cell area. In fact, our results show that due to the plane stress assumptions, an increase in cell's thickness is possible (with increasing out-of-plane deformation) such that the global volume of the cell is preserved.

5.3.3 *Cortical contraction*

In addition to cytoskeletal contraction T^0, contractile cells may change their shape by applying a cortical tension T_s^0. This process is thought to be at the origin of cell blebbing (Tinevez et al. 2009). The last example, therefore, investigates how the application of surface tension T_s^0 triggers changes in cell deformation, as shown in Figure 10.

Results indicate that the application of surface tension tends to decrease surface curvature, and that this effect is increasingly pronounced as surface stiffness decreases. In the case of high surface stiffness, surface tension has a

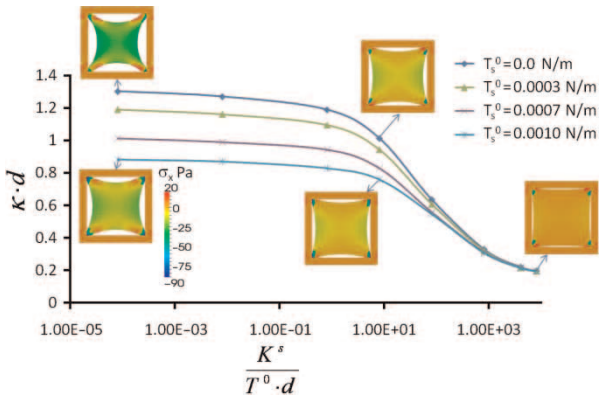

Figure 10. Effect of cortical contraction (surface tension) on the normalised curvature of the cortical membrane.

small effect on cortical deformation and thus becomes negligible on the general deformation of the cell. These trends can be explained by viewing the tensed cortical membrane as a cable that is straightened by applying an axial force on its two ends. In a similar way, surface tension works to make the cortical membrane return to its original straight line, providing an efficient way for the cell to control its shape through active cortical contraction.

6. Summary and conclusions

In summary, this paper presented a new theoretical/computational framework to model the large deformation of cells, accounting for the effect of a stiff surrounding cortical membrane. Under the assumption of a very small cortical thickness, we developed the equations of surface elasticity, originally developed for free surface stresses in solids, in the case of large deformations following the Eulerian description. A numerical formulation, based on the XFEM/level-set method, was then introduced and utilised to study the effect of cortical elasticity on the deformation of a contractile cell. The contributions and advantages of the proposed method can be summarised as follows:

(1) the geometry of the cell is entirely represented by level-set functions that are defined independently from the finite element mesh. Simple, regular FEM meshes may, thus, be used regardless of the geometric complexity of the cell;
(2) discontinuities in velocities and deformations resulting from the governing equations are naturally taken into account within the XFEM methodology and
(3) the model provides an efficient and flexible way to incorporate the contribution of cortical membrane in cell mechanics. In particular, it can easily be extended to incorporate more sophisticated descriptions of the cell's cytoskeleton and its cortical membrane.

Our analysis on the effects of the cortical membrane on cell deformation generally showed that by adding stiffness to the cell's surface, the presence of the cortex induced homogeneous membrane strains and curvature. Although this aspect had been shown with a simple analysis considering a cable deforming under the action of an external perpendicular force, the model neglected the effects of cytoskeletal elasticity on surface deformation. Because it is able to incorporate the effect of both cytoskeleton and cortical membrane deformation, the proposed framework could overcome these limitations and accurately capture the distinct role of surface and bulk elasticity in cell deformation. Results showed that although the analytical solution provides a good approximation of membrane curvature when the cytoskeleton is much softer than the cortical membrane, it greatly overestimated its value for low values of cortical stiffness. The numerical method was then used to investigate the variation of cell deformation for various cytoskeletal elastic parameters as well as cortical tension and elasticity. This technique may, therefore, prove very useful in the determination of cell properties through the analysis of its shape. Besides this, the proposed framework establishes a fast and efficient method that can accurately account for cortical elasticity in future research on cell contraction, migration and cell-matrix interactions.

Acknowledgements

The authors would also like to thank the National Science Foundation, grant number CMMI-0900607 in support for this work.

References

Ateshian G, Likhitpanichkul M, Hung C. 2006. A mixture theory analysis for passive transport in osmotic loading of cells. J Biomech. 39:464–475.
Bar-Ziv R, Tlusty T, Moses E, Safran SA, Bershadsky A. 1999. Pearling in cells: A clue to understanding cell shape. Proc Natl Acad Sci. 96:10140–10145.
Belytschko T, Gracie R. 2007. On XFEM applications to dislocations and interfaces. Int J Plast. 23(10–11):1721–1738.
Belytschko T, Liu WK, Moran B. 2000. Nonlinear finite elements for continua and structures. Chichester, West Sussex, England: John Wiley & Sons.
Belytschko T, Parimi C, Moes N, Sukumar N, Usui S. 2003. Structured extended finite element methods for solids defined by implicit surfaces. Int J Numer Methods Eng. 56(4):609–635.
Bischofs IB, Klein F, Lehnert D, Bastmeyer M, Schwuartz US. 2008. Filamentous network mechanics and active contractility determine cell and tissue shape. Biophys J. 95:3488–3496.
Butcher D, Alliston T, Weaver V. 2009. A tense situation: forcing tumour progression. Nat Rev Cancer. 9:108–122.
Dai J, Sheetz M. 1999. Membrane tether formation from blebbing cells. Biophys J. 77:3363–3370.
Deshpande VS, McMeeking RM, Evans AG. 2006. A bio-mechanical model for cell contractility. Proc Natl Acad Sci. 103(38):14015–14020.

Dolbow J, Belytschko T. 1999. Finite element method for crack growth without remeshing. Int J Numer Methods Eng. 46(1): 131–150.

Dolbow J, Moes N, Belytschko T. 2001. An extended finite element method for modeling crack growth with frictional contact. Comput Methods Appl Mech Eng. 190(51–52): 6825–6846.

Fackler O, Grosse R. 2008. Cell motility through plasma membrane blebbing. J Cell Biol. 181:879–884.

Farsad M, Vernerey F, Park H. 2010. An extended finite element/level set method to study surface effects on the mechanical behavior and properties of nanomaterials. Int J Numer Methods Eng (www.interscience.wiley.com) DOI: 10.1002/nme.2946.

Guilak F, Erickson G, Ping Ting-Beall H. 2002. The effects of osmotic stress on the viscoelastic and physical properties of articular chondrocytes. Biophys J. 82:720–727.

Gurtin ME. 1998. A general theory of curved deformable interfaces in solids at equilibrium. Philos Mag A. 78(5): 1093–1109.

Hansen JC, Skalak R, Chien S, Hoger A. 1996. An elastic network model based on the structure of the red blood cell membrane skeleton. Biophys J. 70:146–166.

Hansen JC, Skalak R, Chien S, Hoger A. 1997. Influence of network topology on the elasticity of the red blood cell membrane skeleton. Biophys J. 72:2369–2381.

Harris A, Stopak D, Wild P. 1980. Fibroblast traction as a mechanism for collagen morphogenesis. Nature. 290:249–251.

Hartwig JH, Shevlin P. 1986. The architecture of actin filaments and the ultrastructural location of actin-binding protein in the periphery of lung macrophages. J Cell Biol. 103:1007–1020.

Hettich T, Hund A, Ramm E. 2008. Modeling of failure in composites by X-FEM and level sets within a multiscale framework. Comput Methods Appl Mech Eng. 197:414–424.

Hogan MJ, Feeney L. 1963. The ultrastructure of the retinal vessels: III. Vascular-Glial relationships. J Ultra Res. 9: 47–64.

Ingber D. 2003a. Tensegrity I. Cell structure and hierarchical systems biology. J Cell Sci. 116:1157–1173.

Ingber D. 2003b. Tensegrity II. How structural networks influence cellular information processing networks. J Cell Sci. 116:1397–1408.

Keller H, Eggli P. 1998. Actin accumulation in pseudopods or in the tail of polarized walker carcinosarcoma cells quantitatively correlates with local folding of the cell surface membrane. Cell Motil Cytoskeleton. 40:342–353.

Levental I, Georges P, Janmey P. 2006. Soft biological materials and their impact on cell function. Soft Matter. 2:1–9.

MacKintosh F, Kas J, Janmey P. 1995. Elasticity of semi flexible biopolymer networks. Phys Rev Lett. 75:4425.

Moes N, Cloirec M, Cartraud P, Remacle JF. 2003. A computational approach to handle complex microstructure geometries. Comput Methods Appl Mech Eng. 192:3163–3177.

Mohammadi S. 2008. Extended finite element method. Chichester, West Sussex, England: John Wiley & Sons.

Schwarz U, Bischofs I. 2005. Physical determinants of cell organization in soft media. Med Eng Phys. 27:763–772.

Stamenovic D, Fredberg J, Wang N, Butcher D, Ingber D. 1996. A microstructural approach to cytoskeletal mechanics based on tensegrity. J Theor Biol. 181:125–136.

Stehbens WE. 1966. The basal attachment of endothelial cells. J Ultra Res. 15:389–399.

Tinevez JY, Schulze U, Salbreux G, Roensch J, Joanny J, Paluch E. 2009. Role of cortical tension in bleb growth. PNAS. 106:18581–18586.

Unnikrishnan GU, Unnikrishnan VU. 2007. Constitutive material modeling of cell: A micromechanics approach. J Biomech Eng. 129:315–323.

Vernerey F, Liu W, Moran B. 2007. Multi-scale micromorphic theory for hierarchical materials. J Mech Phys Solids. 55: 2603–2651.

Vernerey FJ, Liu W, Moran B, Olson G. 2007. A micromorphic model for the multiple scale failure of heterogeneous materials. J Mech Phys Solids. 56(4):1320–1347.

Vernerey F, Liu W, Moran B, Olson G. 2009. Multi-length scale micromorphic process zone model. Comput Mech. 44: 45–51.

Wang H, Dembo M, Wang Y. 2000. Substrate flexibility regulates growth and apoptosis of normal but not transformed cells. Am J Physiol Cell Physiol. 279:C1345–C1350.

Wang N, Naruse K, Stamenovic D, Fredberg J, Mijallovich S, Tolic-Nørrelykke I, Polte T, Mannix R, Ingber D. 2001. Mechanical behavior in living cells consistent with the tensegrity model. PNAS. 98(14):7765–7770.

Yvonnet J, Quang HL, He QC. 2008. An XFEM/level set approach to modelling surface/interface effects and to computing the size-dependent effective properties of nanocomposites. Comput Mech. 42:119–131.